Article

Modeling, Simulation and Control Strategy Optimization of Fuel Cell Hybrid Electric Vehicle

Umidjon Usmanov [1],* , Sanjarbek Ruzimov [1] , Andrea Tonoli [2] and Akmal Mukhitdinov [3]

1   Mechanical and Aerospace Engineering Department, Turin Polytechnic University in Tashkent,
    Tashkent 100095, Uzbekistan; sanjarbek.ruzimov@polito.it
2   Department of Mechanical and Aerospace Engineering (DIMEAS), Politecnico di Torino, 10129 Turin, Italy;
    andrea.tonoli@polito.it
3   Department of Vehicle Engineering, Tashkent State Transport University, Tashkent 100047, Uzbekistan;
    akmalmukhitdinov@gmail.com
*   Correspondence: usmanovumidjoni@gmail.com; Tel.: +998-903183767

Abstract: This work represents the development of a Fuel Cell Hybrid Electric Vehicle (FCHEV) model, its validation, and the comparison of different control strategies based on the Toyota Mirai (1st generation) vehicle and its subsystems. The main investigated parameters are hydrogen consumption, and the variation of the state of charge, current, and voltage of the battery. The FCHEV model, which is made up of multiple subsystems, is developed and simulated in MATLAB® Simulink environment using a rule-based control strategy derived from the real system. The results of the model were validated using the experimental data obtained from the open-source Argonne National Laboratory (ANL) database. In the second part, the equivalent consumption minimization strategy is implemented into the controller logic to optimize the existing control strategy and investigate the difference in hydrogen consumption. It was found that the ECMS control strategy outperforms the rule-based one in all drive cycles by 0.4–15.6%. On the other hand, when compared to the real controller, ECMS performs worse for certain considered driving cycles and outperforms others.

Keywords: fuel cell; fuel cell hybrid electric vehicles; backward modeling; Toyota Mirai; control strategy; rule-based control; equivalent consumption minimization strategy

1. Introduction

One of the main global problems in recent years is climate change (global warming). According to the report of the United States Environmental Protection Agency (EPA), the transportation sector is responsible for the largest share of greenhouse gas emissions (29% of 2019 greenhouse gas emissions) [1]. Therefore, authorities and environmental agencies establish strict limitations for automotive manufacturers concerning carbon dioxide gas emissions. Currently, the automotive industry mainly depends on fossil fuels, although world oil reserves have been estimated at 50 years of contemporary consumption [2]. Thus, the transportation industry is being asked for the implementation of a decarbonization program or at least the reduction of greenhouse gas emissions [3,4]. The realization of these tasks with the conventional propulsion system is challenging. Hybridization of the existing driving system with an additional energy source, such as batteries or supercapacitors, is one solution [5]. The combination of electric and conventional propulsion systems allows for the significant reduction of greenhouse CO_2 emissions. In spite of the popularity of this solution, it is impossible to reach zero carbon emissions. Hydrogen as an energy carrier for the propulsion of vehicles is seen as a solution for sustainable green mobility [6] with higher energy density than electric batteries, with water as the only exhaust product.

Lately, the implementation of fuel cell vehicles in the transportation sector has emerged as a solution [7]. Hydrogen as an energy carrier makes it possible to have tank-to-wheel carbon-free propulsion and allows it to cover basic driving requirements. In the fuel

cell system, hydrogen gas combined with oxygen from ambient air produces electricity, which is used for the propulsion, heat, and pure water [8]. However, the fuel cell system as the only power supply has lower power density and slower power response when compared with ICE [7]. The usage of an additional energy storage system composed of batteries or super-capacitors coupled with such a system allows us to tackle this issue and creates several benefits. This solution makes it possible for energy recovery from braking, a more flexible energy supply, prolongs the life of the fuel cell system, and minimizes the consumption of hydrogen [9]. In addition, fuel cells (FCs) are three times more efficient than the ICE and are advantageous in terms of driving range and refueling time compared with pure battery electric vehicles (BEV) [10–12]. In many cases, the fuel cell system is designed to provide the average power demand while an additional energy source is used to provide the transient power demand to supplement the insufficient power of FC during power-starving phases such as acceleration or climbing [13].

The possible configurations of a fuel cell vehicle (FCV) are (1) FCV—a pure fuel cell vehicle (without additional electrical energy storage), and (2) FCHEV—a fuel cell hybrid electric vehicle (solution with a battery or super-capacitor coupled with the fuel cell through DC/DC converter) [14]. The second one is also referred to as the Series hybrid-fuel cell configuration [15]. As mentioned above, due to the delayed power response of FC, the implementation of batteries or super-capacitors may increase the efficiency of the FC stack and allow regenerative braking. FC vehicles with super-capacitors are more efficient in absorbing regenerative power than batteries due to the high power density of super-capacitors and providing it during power starving phases. However, the energy density of super-capacitors is much lower than that of batteries. The realization of these solutions can be found in the Honda FCX Clarity and Toyota Mirai [16].

Since FCHEV has two on-board energy storage devices, the problem of energy management arises. An energy management system (EMS) aims to reduce fuel usage while preserving the battery state of charge (SOC) and extending the battery life [17,18]. The key role of EMS for FCHEV is to decide on the power splitting for energy sources at any given time while maintaining the vehicle driveability constraints [18]. The equivalent consumption minimization strategy (ECMS) is one of the most widely used EMS and it is based on the conversion of electrical energy in the energy storage sources into equivalent fuel consumption and minimization of the cost function. The latter is composed of the instantaneous fuel consumption and equivalent fuel consumption of the electric drive [18,19]. In this strategy, all energy of the vehicle comes directly or indirectly from hydrogen. The charging and discharging of batteries or super-capacitors should be equivalent to hydrogen consumption according to the set of equivalence factors. The energy consumption of both the electric drive and FC system should be equivalent to hydrogen consumption in order to minimize the system's instantaneous fuel utilization [20]. The calculation of the equivalent fuel consumption of batteries is performed by assuming that SOC variation is virtually compensated by the FC system. This principle was first introduced by Paganelli et al. [21], who presented an algorithm for the EMS of HEV that chooses the power split between an electric motor and an engine to minimize fuel consumption. As a result, 17.5% of fuel reduction was achieved in the simulation. Concerning the implementation of ECMS on FCHEV, several works were carried out by researchers. Paganelli et al. [22] proposed an ECMS control strategy for real-time application of an instantaneous power split between a fuel cell and an electrical accumulator in a charge-sustaining fuel cell hybrid vehicle and allowing the overall minimization of hydrogen consumption while meeting the driver demand. Han et al. [23] studied the performance of a dynamic programming control strategy, comparing it with Pontryagin's minimum principle and ECMS. Liu et al. [20] proposed ECMS to solve the power allocation problem of FCHEV in order to reduce hydrogen energy consumption and prolong battery life. As a result, the optimal output power of FC was obtained by using ECMS, and the battery output power was smoothed, achieving the best power distribution between the battery and the super-capacitor. Bassam et al. [24] simulated different control strategies, including ECMS on hybrid fuel cell/battery passenger

vessels. An optimized proportional-integral (PI) controller-based energy management strategy was presented. They made a comparative analysis with the original PI controller, ECMS, and state-based energy management strategies in terms of hydrogen consumption and FC stresses with no additional hardware changes. Li et al. [25] designed an ECMS strategy for the FCHEV powered by a fuel cell, battery and super-capacitor. FC system operates at its best efficiency zone and the battery is used as a long-term energy buffer, while the super-capacitor supplies the peak power. Kamal et al. [26] presented a comparative analysis of the performance of different energy management strategies, including ECMS simulation over the UDDS driving cycle.

In this context, the present paper aims to compare three control strategies; namely, rule-based, optimization-based equivalent consumption minimization strategy, and the real control strategy used in Toyota Mirai. In the first part of the paper, the modeling, simulation, and validation of FCHEV based on the Toyota Mirai (1st generation) vehicle are presented. For this purpose, various subsystems of the vehicle are developed with mathematical relations, and proper block diagrams are constructed by means of backward modeling approaches. The obtained results are compared with experimental data from the open-source Argonne National Laboratory database [27,28]. In the second part, the ECMS control strategy is implemented and replaced Toyota Mirai's real control strategy in order to optimize hydrogen consumption and compare with the results obtained using experimental and rule-based energy management strategies over various driving cycles. Finally, the hydrogen economy optimization windows are determined and proper conclusions are made concerning the performance of control strategies for different driving patterns.

2. Methodology

For the Toyota Mirai, the fuel cell stack works as a primary power source, while the battery works as an auxiliary source or power buffer [29]. The backward modeling technique is employed during this research, meaning that input parameters for the model come from the driving cycle, which are WLTC, NEDC, UDDS, JC08, HWY, and US06 in our case, and the output parameters are hydrogen consumption and battery SOC, while in reality, the situation is inverse. In this research paper, the total system is subdivided into several subsystems, which are the vehicle, speed reducer, electric machine, power control unit, battery, boost converter, fuel cell system, and hydrogen tanks. The general configuration of the system is provided in Figure 1.
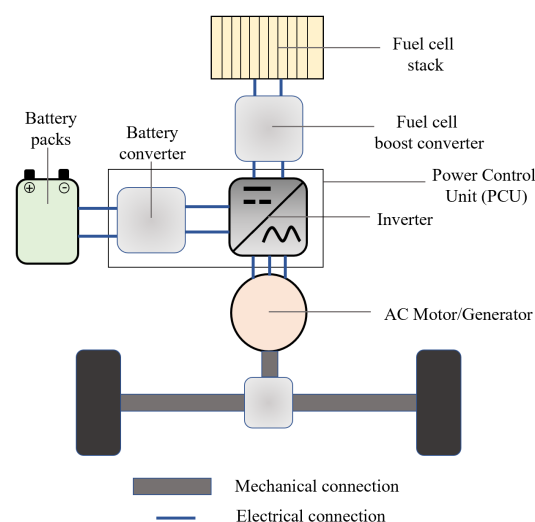
Figure 1. Toyota Mirai FCHEV configuration [30,31].

2.1. Vehicle Dynamics Subsystem

This subsystem aims at calculating the angular velocity and torque of a driving axle given the acceleration and velocity request from the driving cycle [32]. The equations of

this block are the equations of the longitudinal dynamics of a vehicle. The total tractive force at a tire-ground contact is the sum of all resistance forces and the inertia force due to acceleration [32,33].

$$\omega_{wh} = \frac{v}{r_{wh}} \tag{1}$$

$$T_{wh} = \left(\frac{1}{2} \cdot \rho \cdot v^2 \cdot A_f \cdot C_d + f_r \cdot M \cdot g + M \cdot g \cdot \sin\theta + M \cdot a_x\right) \cdot r_{wh} + 4 \cdot J_{wh} \cdot \alpha_{wh} \tag{2}$$

$$\alpha_{wh} = \frac{a_x}{r_{wh}} \tag{3}$$

where T_{wh}—torque of the wheels, [Nm]; ω_{wh}—wheel angular velocity, [rad/s]; α_{wh}—wheel angular acceleration, [rad/s^2]; g—gravity constant, [m/s^2]; r_{wh}—radius of the wheel, [m]; J_{wh}—rotational inertia of the wheel, [kgm^2]; ρ—air density, [kg/m^3]; v—vehicle speed, [m/s]; A_f—vehicle frontal area, [m^2]; C_d—aerodynamic drag coefficient, [-]; f_r—rolling resistance coefficient, [-]; M—FCHEV's total mass with full load, [kg]; θ—road inclination, [deg]; a_x—longitudinal acceleration, [m/s^2].

The values of vehicle and powertrain parameters are listed in Table 1. The impact of the lateral dynamics is not taken into account, and the additional torque due to the inertia of rotating parts is considered separately for each part of the vehicle and included in the mathematical model of the corresponding part.

Table 1. Parameters of Toyota Mirai FCHEV used in calculation [34].

Parameters	Label	Unit	Value
Vehicle total mass	M	kg	1927
Aerodynamic drag coefficient	C_d	-	0.29
Air density	ρ	kg/m^3	1.2
Vehicle frontal area	A_f	m^2	2.23
Rolling resistance coefficient	f_r	-	0.01
Wheel radius	r_{wh}	m	0.316
Wheel inertia	J_{wh}	kgm^2	0.32
Reduction ratio	τ	-	9.09
Speed reducer efficiency	η_{sr}	-	0.98
Auxiliary power	P_{aux}	W	440

2.2. Speed Reducer Subsystem

This subsystem calculates the torque and speed request for the electric motor given the torque and speed of the wheels and the reduction ratio. The Toyota Mirai FCHEV is equipped with a single-speed reducer ratio. Therefore, the electric machine torque will be equal to

$$\omega_{em} = \omega_{wh}\tau \tag{4}$$

$$\alpha_{em} = \alpha_{wh}\tau \tag{5}$$

$$T_{em} = \begin{cases} \frac{T_{wh}}{\tau \eta_{sr}} & T_{wh} > 0 \qquad \text{Traction mode} \\ \frac{T_{wh}\eta_{sr}}{\tau} & T_{wh} < 0 \quad \text{Regeneration mode} \end{cases} \tag{6}$$

where τ—reduction ratio, [-]; η_{sr}—speed reducer efficiency, [-]; ω_{em}—electric machine angular velocity, [rad/s]; α_{em}—electric machine angular acceleration, [rad/s^2].
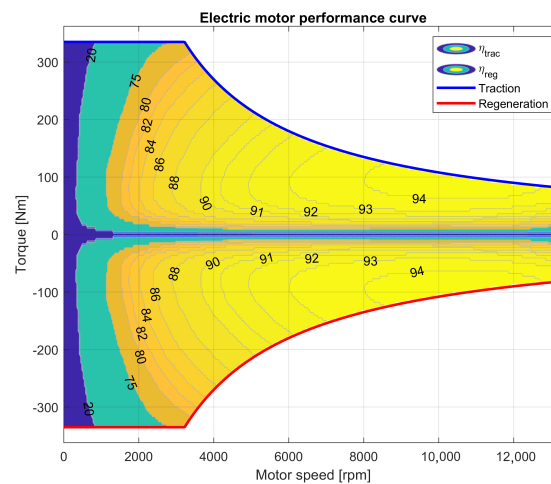
2.3. Electric Machine Subsystem

Transmission system power request and electric machine efficiency can be used to compute power supply to an electric machine.

$$P_{\text{req}} = \begin{cases} \frac{(T_{em}+J_{em}\alpha_{em})\omega_{em}}{\eta_{em}} + P_{aux} & \text{Traction} \\ (T_{em}+J_{em}\alpha_{em})\omega_{em}\eta_{em} + P_{\text{aux}} & \text{Regeneration} \end{cases} \tag{7}$$

where P_{req}—power required by batteries and fuel cell system, [W]; J_{em}—electric machine inertia, [kgm^2]; η_{em}—electric machine efficiency, [-]; P_{aux}—auxiliary power, [W].

Electric machine efficiency depends on its torque and speed, and is graphically represented in the electric machine efficiency map. An AC synchronous motor with a maximum power of 113 kW and maximum torque of 335 Nm is used in the 2014 Toyota Mirai FCHEV [34]. Due to the unavailability of this motor efficiency map, a similar motor with almost the same peak power and torque is considered, specifically, a YASA P400 R SERIES AC synchronous motor's efficiency map [35] is used, and the parameters are re-scaled to fit the peak torque and speed [36]. The final representation of the efficiency map and torque curve of the electric machine is illustrated in Figure 2.


Figure 2. Electric machine efficiency map [35].

2.4. Fuel Cell System Model

The full onboard fuel cell system is made of a fuel cell stack and auxiliary systems such as hydrogen, air, water, coolant, and electrical supply circuits [29]. The full model requires additional computing time since it includes intricate internal dynamic responses [37]. Due to the intricacy of the FC model, this paper focuses mostly on the power distribution of the bus rather than the precise FC conversion process. Consequently, a simple efficiency graph, which is obtained from the experimental results, is used for the simulation.

The experimental data, publicly available from the Argonne National Laboratory [28], were used to establish the FC model. The curves for the hydrogen flow rate, FC stack efficiency, FC system efficiency, and polarization curve have been reconstructed from the experimental data. The experimental operating points and the dependence of FC stack and system efficiency, and hydrogen flow rate on the FC output power have the form illustrated in Figure 3.
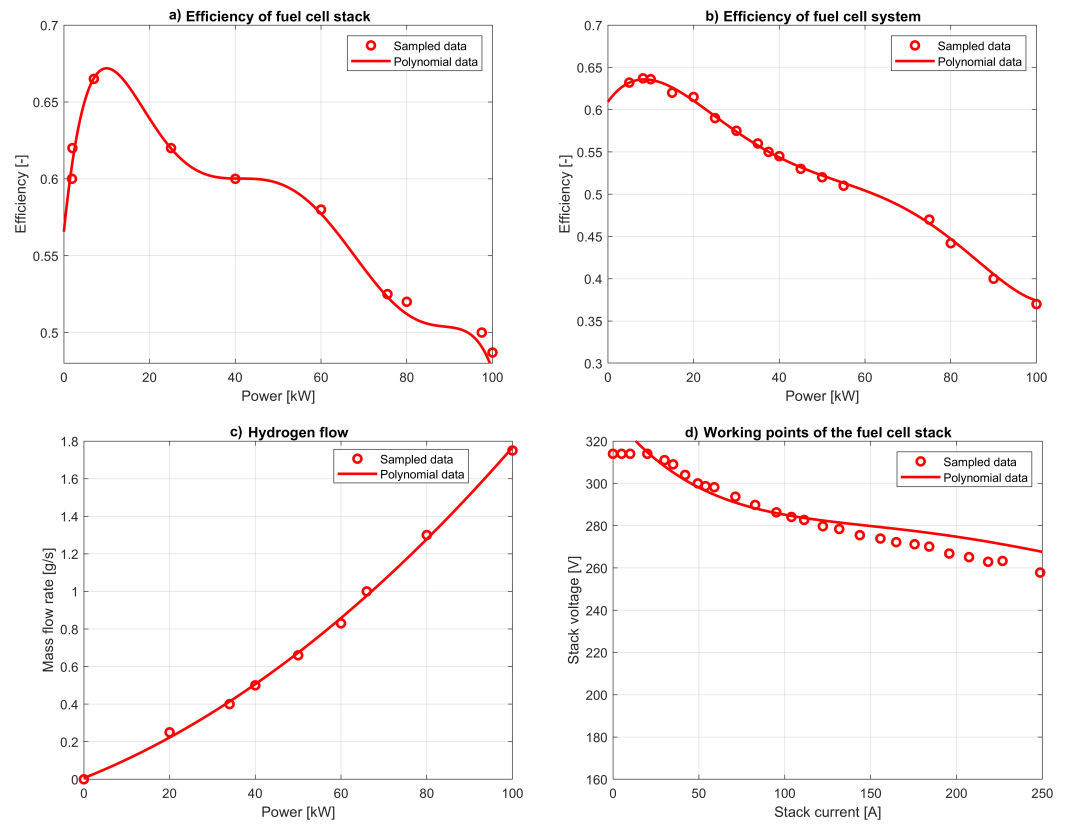
Figure 3. Fuel cell system characteristics [28]: (**a**) FC stack efficiency, (**b**) FC system efficiency, (**c**) hydrogen flow, and (**d**) polarization curve.

Consequently, this dependence can be approximated with polynomials of the sixth degree for FC stack efficiency, the fifth degree for FC system efficiency, and the second degree for hydrogen flow rate, as shown in Equations (8)–(10).

$$\eta_{stack} = k_1 \cdot P^6 + k_2 \cdot P^5 + k_3 \cdot P^4 + k_4 \cdot P^3 + k_5 \cdot P^2 + k_6 \cdot P + k_7 \tag{8}$$

where $k_1 = -3.322 \cdot 10^{-11}; k_2 = 1.08 \cdot 10^{-8}; k_3 = -1.343 \cdot 10^{-6}; k_4 = 7.986 \cdot 10^{-5}; k_5 = -2.3 \cdot 10^{-3}; k_6 = 2.69 \cdot 10^{-2}; k_7 = 0.56$.

$$\eta_{sys} = a_1 \cdot P^5 + a_2 \cdot P^4 + a_3 \cdot P^3 + a_4 \cdot P^2 + a_5 \cdot P + a_6 \tag{9}$$

where $a_1 = 4.94 \cdot 10^{-10}; a_2 = -1.357 \cdot 10^{-7}; a_3 = 1.335 \cdot 10^{-5}; a_4 = 5.658 \cdot 10^{-4}; a_5 = 7.05 \cdot 10^{-3}; a_6 = 0.6092$.

$$\dot{m}_{H_2} = b_1 \cdot P^2 + b_2 \cdot P + b_3 \tag{10}$$

where $b_1 = 8.5 \cdot 10^{-5}; b_2 = 9.1 \cdot 10^{-3}; b_3 = 0.0064$.

By using the FC polarisation curve (Figure 3d), the fuel cell stack current can be determined. The dependence of the stack voltage and stack current can be approximated with the polynomial of the fifth degree:

$$V_{stack} = c_1 \cdot I^5 + c_2 \cdot I^4 + c_3 \cdot I^3 + c_4 \cdot I^2 + c_5 \cdot I + c_6 \tag{11}$$

where $c_1 = -4.587 \cdot 10^{-11}; c_2 = 6.67 \cdot 10^{-8}; c_3 = -3.553 \cdot 10^{-5}; c_4 = 0.0085; c_5 = -1.028; c_6 = 332.2$.

2.5. Battery Model

A nickel metal hydride battery pack with a capacity of 6.5 Ah is used in the 2014 Toyota Mirai as an additional to the FC power source [34]. By integrating a battery pack into the propulsion system, regenerative braking is made possible, and the vehicle's autonomy is increased. From the standpoint of energy management, the majority of batteries are modeled using a Thevenin equivalent circuit model [32,33]. The data from the 2004 Toyota Prius, experimentally obtained by Idaho National Laboratory (INL) and made publicly available through their website [38], which has the closest battery data, are used.

The battery cell characteristics are maintained while being adjusted to the battery pack nominal parameters given by Toyota Mirai datasheets. An ideal voltage source, internal charging, and discharging resistances are the three elements of this model (Figure 4). The open circuit voltage (OCV) of the battery is represented by the ideal voltage source and is dependent on the SOC of the battery (Figure 5a). The terminal voltage, battery internal charging, and discharging resistances are represented as V_{term}, R_{ch}, and R_{dch}, respectively, and are also the functions of the battery SOC. Figures 5b,c demonstrate this dependence. The charging and discharging currents are I_{ch} and I_{dch}, respectively. Internal resistances and open circuit voltage depend on SOC and temperature. In this work, the dependence on temperature is not taken into account and the temperature is assumed to be constant. These relations can be approximated with the polynomial of the fifth degree for battery OCV, and fourth degree for battery charging and discharging resistances.

$$OCV = m_1 \cdot SOC^5 + m_2 \cdot SOC^4 + m_3 \cdot SOC^3 + m_4 \cdot SOC^2 + m_5 \cdot SOC + m_6 \quad (12)$$
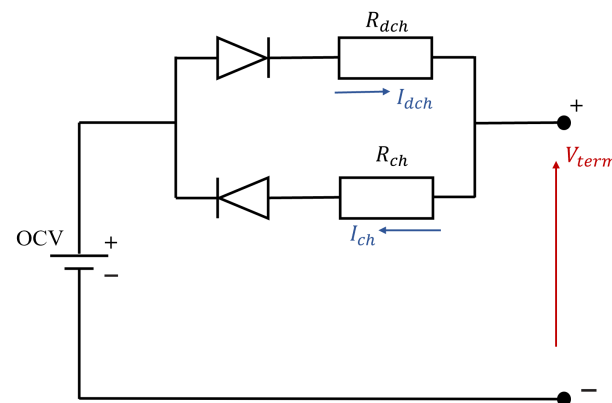
where $m_1 = 1722.4$; $m_2 = -4747.5$; $m_3 = 4891.9$; $m_4 = -2312.1$; $m_5 = 525.72$; $m_6 = 200.06$.

$$R_{ch} = n_1 \cdot SOC^4 + n_2 \cdot SOC^3 + n_3 \cdot SOC^2 + n_4 \cdot SOC + n_5 \quad (13)$$

where $n_1 = 0.0056$; $n_2 = -0.0254$; $n_3 = 0.0372$; $n_4 = -0.0203$; $n_5 = 0.0223$.

$$R_{dch} = q_1 \cdot SOC^4 + q_2 \cdot SOC^3 + q_3 \cdot SOC^2 + q_4 \cdot SOC + q_5 \quad (14)$$

where $q_1 = 0.0188$; $q_2 = -0.0547$; $q_3 = 0.0765$; $q_4 = -0.0457$; $q_5 = 0.0349$.


Figure 4. Battery equivalent circuit.

The coefficient of correlation (R^2) in all the above equations is within 0.80–0.95, which indicates the acceptable correspondence between the equations and experimental data. The nominal parameters of the battery pack used in the simulation are represented in Table 2. By knowing the power required from the battery P_{bat}, its charging and discharging currents and battery SOC can be formulated from energy and charge conservation principles as follows [18,32]:

$$I_{bat} = \begin{cases} \dfrac{V_{OCV} - \sqrt{V_{OCV} - 4R_{dch} \cdot P_{bat}}}{2R_{dch}} & P_{bat} \geq 0 \\[3mm] \dfrac{-V_{OCV} + \sqrt{V_{OCV} + 4R_{ch} \cdot P_{bat}}}{2R_{ch}} & P_{bat} < 0 \end{cases} \tag{15}$$

$$SOC(t) = \begin{cases} SOC(t - \Delta t) - \dfrac{\int I_{dch}^{k} dt}{Q_{bat}} & P_{bat} \geq 0 \\[3mm] SOC(t - \Delta t) + \dfrac{\int I_{ch} dt}{Q_{bat}} & P_{bat} < 0 \end{cases} \tag{16}$$

where P_{bat}—power required from batteries, [W]; k—coefficient that takes into account Peukert's effect (ranges between 1 and 1.2 for NiMH batteries [39]); $SOC(t)$—battery state of charge at instant time t; $SOC(t - \Delta t)$—battery state of charge one step time before; Q_{bat}—the battery capacity represented in Coulomb, [C].
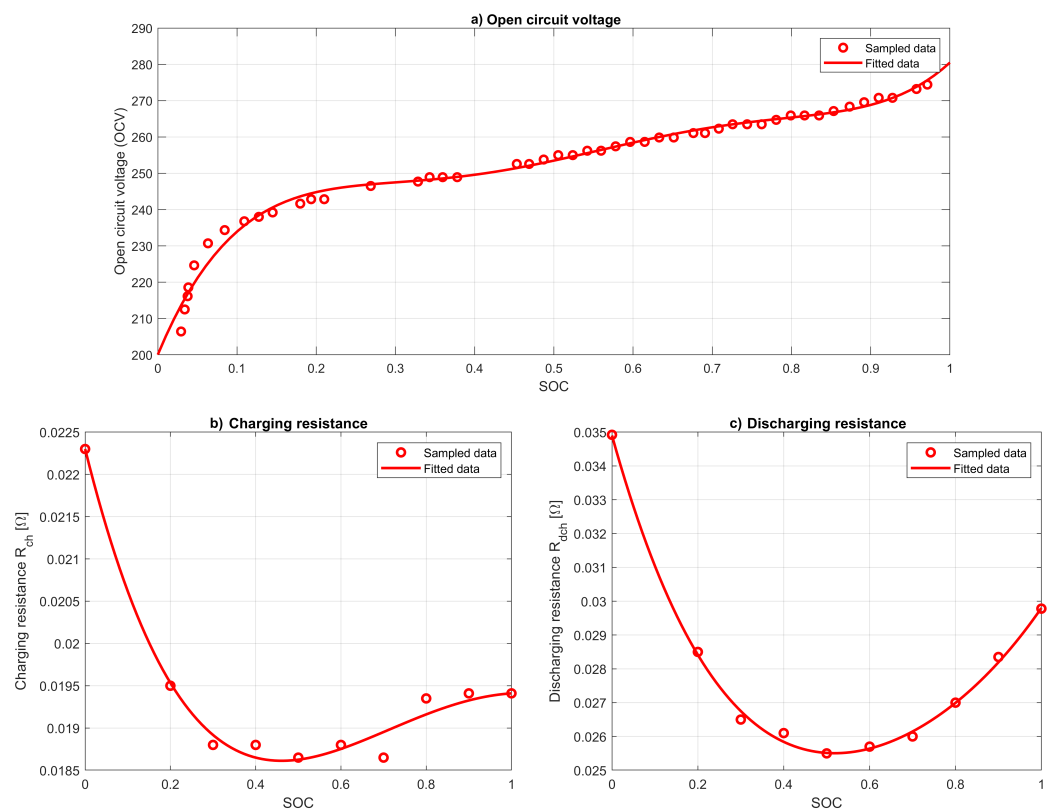
Figure 5. The dependence of battery parameters on SOC [38]: (**a**) open circuit voltage, (**b**) charging resistance, and (**c**) discharging resistance.

Table 2. Specifications of Toyota Mirai FCHEV battery pack [38,40].

Parameters	Unit	Value
Type	-	Air-cooled Nickel Metal Hydride
Nominal capacity	kWh	1.6
Nominal voltage	V	245
Capacity	Ah	6.5
Number of series connections	-	34
Number of parallel connections	-	1

2.6. Boost Converter and Inverter Model

In our case, a boost converter must be integrated in order to step-up the voltage of the fuel cell stack because the voltage that should be given to the AC synchronous motor is approximately 650 V, but the voltage of the FC stack is roughly its nominal value (245 V) [41]. These subsystems' average 95% efficiency is taken into account in the model.

2.7. Energy Management Strategy (EMS) Model

There is flexibility in the power distribution between the fuel cell stack and battery because there are two energy sources. For the optimal realization of EMS, hydrogen consumption should be reduced while battery operates in charge-sustaining mode. The main logic of the power control unit is to force the fuel cell stack to work at high-efficiency points along the optimum operating line in order to reduce hydrogen consumption while the battery supplies the differential power since the efficiency of the fuel cell stack is not constant and strongly depends on power. The value of the SOC of the battery has an impact on the power splitting as well. Only when the SOC exceeds a predetermined threshold value is the battery allowed to supply power.

By using experimental data from the Argonne National Laboratory [28], it is possible to approximate the Toyota Mirai's (1st generation FCHEV) energy management strategy. The choice of power distribution between a fuel cell stack and the battery is heavily influenced by the state of charge (SOC) and the power required by an electric machine. The working points of the FC and battery over WLTC driving cycles are represented as a function of the electric machine's required power and battery SOC, which are illustrated in Figure 6a and as a function of required power only (the planar projection of Figure 6a), which is illustrated in Figure 6b. In Figure 6b, the low values or the high values of SOC mean the values, lower or higher or equal than 57%, respectively. Experimental EMS is reconstructed by means of a rule-based strategy and approximated by means of a linear regression procedure (Figure 6c). The FC and battery working point location depends on the EM required power and battery SOC and is assumed to be divided into six different modes. However, as Figure 6a illustrates, the real control strategy could be more complex and presumably represented by fuzzy-logic rules.

Mode 1—Regenerative braking.

FCHEV works in Mode 1 during the energy regeneration phase, when EM supplies negative power and the braking energy is stored in batteries.

$$P_{fc} = 0 \text{ kW}; \ P_{bat} = P_{req} \tag{17}$$

Mode 2—Load Shift.

FCHEV operates in Mode 2 at low power requests ($0 < P_{req} < 7$ kW) and low SOC (<57%). Since the FC efficiency is extremely small at low power outputs (lower than 7 kW), it provides constant power output, while the differential power charges the batteries.

$$P_{fc} = 7 \text{ kW}; \ P_{bat} = P_{req} - 7 \text{ kW} \tag{18}$$

Mode 3—Only battery.

Mode 3 is used at low power requests ($0 < P_{req} < 7$ kW) and high SOC ($\geq 57\%$). The battery provides all the required power, while the FC is turned off.

$$P_{fc} = 0 \text{ kW}; \ P_{bat} = P_{req} \tag{19}$$

Mode 4—FC driving. Low power.

In mode 4, the battery powers only the auxiliary devices, while the FC provides the traction power for any values of the battery SOC in the interval of P_{req} between 7 and 11 kW.

$$P_{fc} = P_{req} - P_{aux}; \ P_{bat} = P_{aux} \tag{20}$$

Mode 5–FC driving. High power and low SOC.

FCHEV operates in Mode 5 at high power requests ($P_{req} > 11$ kW) and low SOC (<57%). All the power requests are provided by the FC, whereas the battery supplies the auxiliary power.

$$P_{fc} = P_{req} - P_{aux}; \; P_{bat} = P_{aux} \tag{21}$$

Mode 5—FC driving. High power and high SOC.

Mode 6 is activated at high power request ($P_{req} > 11$ kW) and at high values of SOC ($\geq 57\%$). Both battery and FC provide the power with a proportion that is assumed to be described by complex linear equations:

$$P_{fc} = \begin{cases} -0.79 \cdot P_{\text{req}} + 19.11; & 11 \leq P_{\text{req}}\,[kW] < 14 \\ 0.5 \cdot P_{\text{req}} + 0.925; & 14 \leq P_{req}[kW] < 16.5 \\ 0.626 \cdot P_{\text{req}} - 1.168; & 16.5 \leq P_{\text{req}}\,[kW] < 20.7 \\ 0.92 \cdot P_{\text{req}} - 7.2; & 20.7 \leq P_{\text{req}}\,[kW] < 23.5 \\ 0.89 \cdot P_{\text{req}} - 7.7285; & P_{\text{req}}\,[kW] \geq 23.5 \end{cases} \tag{22}$$

$$P_{bat} = P_{req} - P_{fc} \tag{23}$$

The coefficient of correlation (R^2) in all the above equations is within 0.80–0.95, which is interpreted as a good correspondence between the equations and experimental data.
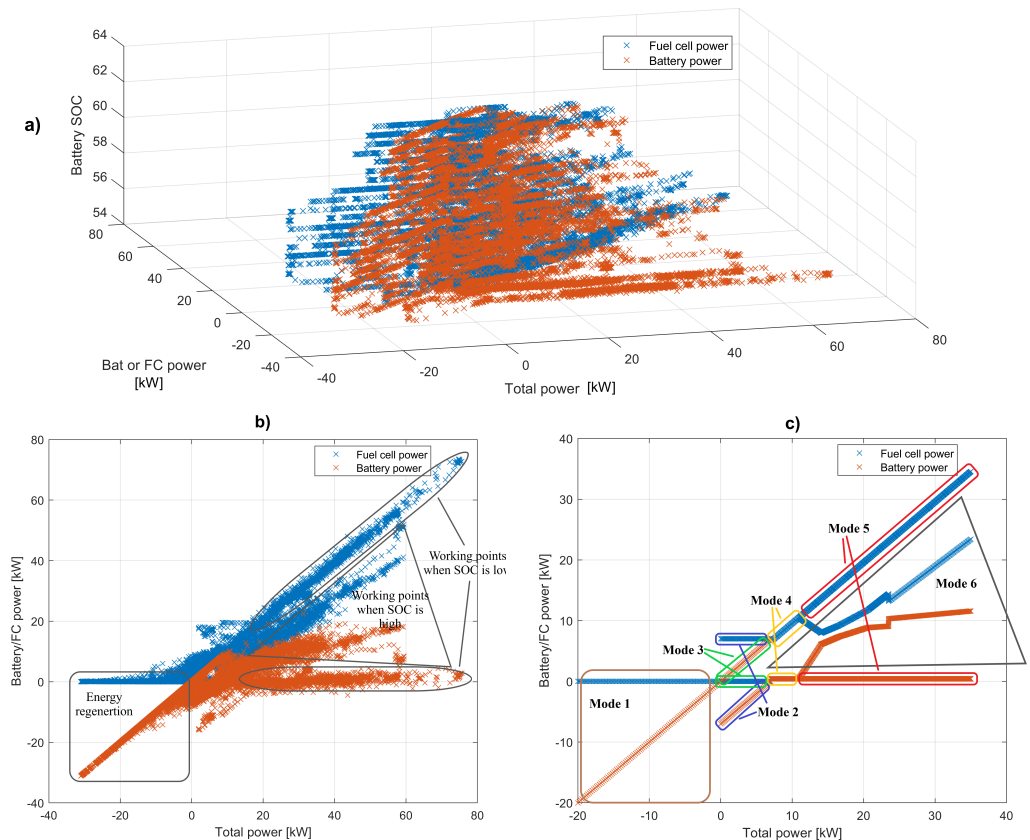
Figure 6. Energy management strategy: (**a**) Experimental working points on WLTC (3-D view) [28], (**b**) experimental working points on WLTC (planar projection), and (**c**) reconstructed rule-based EMS.

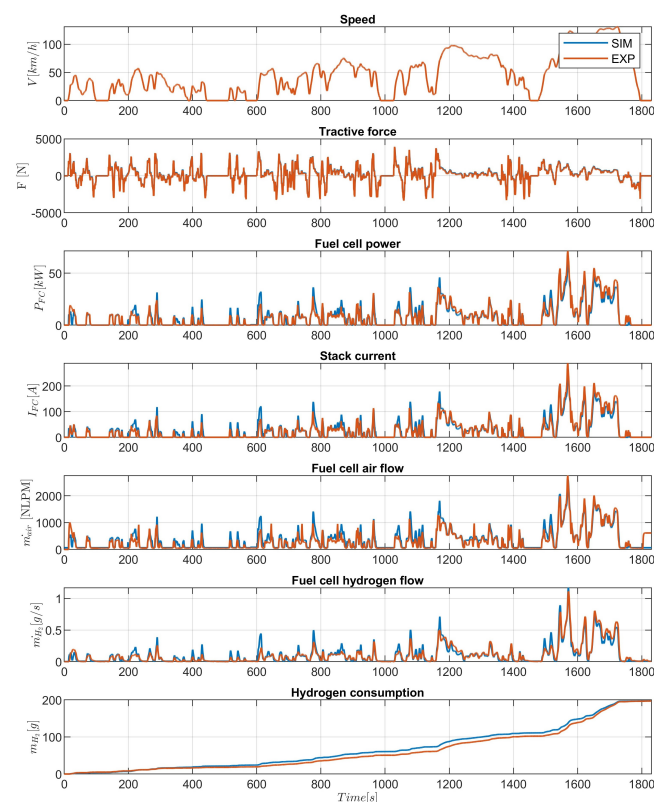## 3. Simulation Results with Rule-Based Control Strategy

The performance of FCHEV using the rule-based control strategy is numerically evaluated in this section. This was performed on the basis of simulations over WLTC, NEDC, UDDS, US06, HWY, and JC08 driving cycles. To focus on the influence of the control

strategy, the variation of the temperature of the powertrain components was not considered in this work. The present model was validated by comparing the simulation results from the MATLAB/Simulink environment with the experimental data from ANL. The ambient temperature indicated in the experimental data of ANL is 22° C (72° F). The reconstructed rule-based control strategy parameters shown in Figure 6c have been used to simulate the performance of the vehicle.

Figures 7 and 8 illustrate speed, tractive force, fuel cell power, fuel cell stack current, fuel cell air flow rate, fuel cell hydrogen flow rate, cumulative hydrogen consumption, electric machine power, battery power, battery current and battery state of charge time history for WLTC, NEDC, UDDS, JC08, US06, and HWY driving cycles. Red lines present the experimental data profile (from ANL data), while blue lines show the simulated. Table 3 summarizes the data for hydrogen consumption and the final value of the battery state of charge and provides information about simulated and experimental cumulative hydrogen consumptions, expressed in grams.

Table 3. Simulation results for hydrogen consumption and battery SOC.

	Hydrogen Consumption [g]					SOC [%]		
Drive Cycle	Simulation	SOC Compensation	Total	Experimental	Difference	Simulation	Experimental	Difference
WLTC	197	0.7	197.7	196.8	**0.5%**	63.29	62.5	**1%**
NEDC	175	2.8	177.8	160.3	**10.9%**	65.62	62.5	**5%**
UDDS	91.4	−1.5	89.9	76.19	**18.1%**	57.37	59	**3%**
JC08	62.5	−5.6	56.9	53.3	**6.7%**	53.31	59.5	**10%**
US06	296	5.2	301.2	323	**6.8%**	62.74	57	**10%**
HWY	201.6	3.1	204.7	243.9	**16.1%**	62	58.5	**6%**

Figure 7. Simulation results with rule-based control strategy for WLTC driving cycle: Fuel cell parameters.
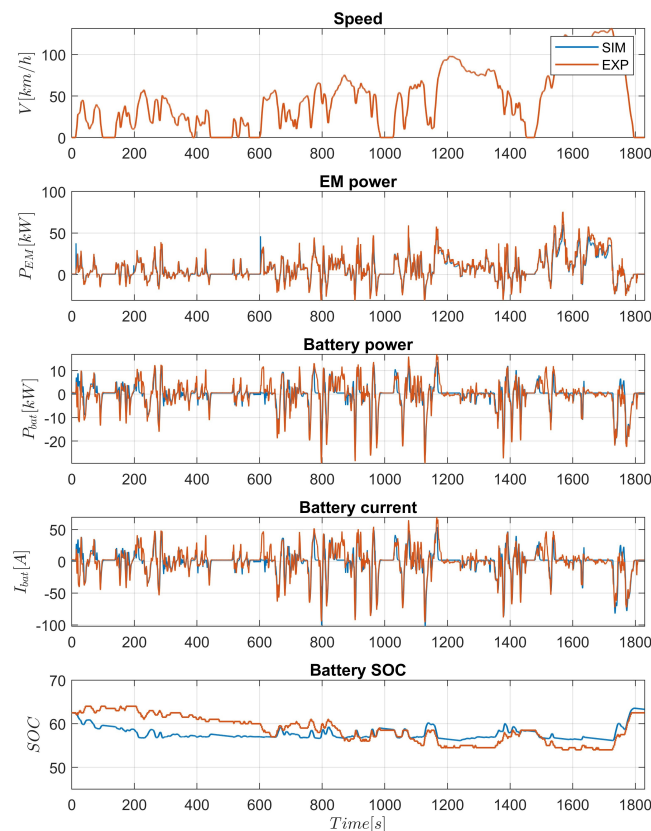
Figure 8. Simulation results with rule-based control strategy for WLTC driving cycle: Battery parameters.

Due to the difference in the simulated and experimental final battery SOC, the corresponding compensation in terms of hydrogen is considered. It was found through an iterative calculating procedure that 0.9 grams of hydrogen equate to the energy content in 1 percent of battery SOC.

The WLTC driving cycle showed the lowest change in the final value of battery SOC, which was found to be 1%, and the highest difference is for the JC08 and US06 cycles, being 10%. Table 3 shows that the highest match between the simulated and experimental data is for the WLTC driving cycle, with a difference of just 0.5%. On the other hand, the UDDS and HWY driving cycles showed the greatest difference between the simulated and experimental overall hydrogen consumption data; 18.1% for UDDS and 16.1% for HWY, respectively. The moderate difference, which is slightly less than 7%, has been noted for JC08 and US06 cycles. The model was actually calibrated by looking at the complete driving cycle, where at low speeds offsets are higher, and lower at high speeds. However, at the driving cycle level, the energy of the simulation and experiments correspond. There are several factors that cause the deviation between simulated and experimental data. One of them is the effect of backward modeling and quasi-static simulation. This methodology does not fully reflect the dynamic behavior since it relies on maps, which are often built during steady-state laboratory testing, neglecting the transients. Another reason is the differences in rules used in EMS (Figure 2) and the EM efficiency map (Figure 6) that do not correspond to the Toyota Mirai EM. Finally, the effect of the dependence of the Peukert coefficient on the discharging current can be highlighted. The derived numerical findings are comparable, and the general shape of the fuel cell and battery parameters are well-reproduced with sufficient accuracy. Given the driving pattern, this mathematical model is used to simulate FCHEV and estimate hydrogen consumption for the comparison of results for the equivalent consumption minimization strategy (ECMS), and the rule-based and experimental control strategies.

4. Equivalent Consumption Minimization Strategy

ECMS logic based on the minimization of equivalent fuel consumption was first proposed by G. Paganelli et al. [21] in order to find local optima for torque split between the electric motor and ICE. For hybrid electric vehicles, it minimizes the overall fuel and electrical energy consumption. The same logic can be implemented for FCHEV in order to determine the best power split between the fuel cell and the battery powers [20].

4.1. ECMS Modeling Methodology

The equivalent hydrogen consumption due to the power provided by the battery is considered by taking into account all the intermediate power flow path efficiencies. Finally, the total hydrogen consumption is the sum of the fuel cell and equivalent battery hydrogen consumption [21],

$$\dot{m}_{eqv} = \dot{m}_{fc}\left(P_{fc}(t)\right) + S_{soc}\dot{m}_{bat}(P_{bat}(t)) \tag{24}$$

where $\dot{m}_{eqv}$—equivalent (total) hydrogen consumption, [g/s]; $\dot{m}_{fc}$—hydrogen consumption due to fuel cell power demand, [g/s]; $\dot{m}_{bat}$—hydrogen consumption due to battery power demand, [g/s]; S_{soc}—penalty function, which takes into account SOC variation.

Depending on the value of S_{soc}, ECMS decides to utilize battery power more at high values of SOC or less at low values. In [18], it is suggested to take S_{soc} in the following form:

$$S_{soc} = 1 - \left(\frac{SOC(t) - SOC_t}{(SOC_{\max} - SOC_{\min}) \cdot 0,5}\right)^{k_S} \tag{25}$$

where $SOC(t)$—current value; SOC_t—desired value; SOC_{max}—maximum value; SOC_{min}—minimum value; and k_s—constant power.

The hydrogen consumption due to battery power demand is different for the cases of traction or regeneration and can be expressed as follows [18,21]:

$$\dot{m}_{bat} = \begin{cases} \dfrac{P_{bat}}{\eta_{ch}\cdot\eta_{dsch}\cdot\eta_{dc}\cdot\eta_{fc}\cdot LHV} & P_{bat} \geq 0 \\[3mm] \dfrac{P_{bat}\cdot\eta_{ch}\cdot\eta_{dsch}}{\eta_{fc}\cdot\eta_{dc}\cdot LHV} & P_{bat} < 0 \end{cases} \tag{26}$$

where, P_{bat}—battery power, [W]; η_{ch}—charging efficiency; η_{dsch}—discharging efficiency; η_{dc}—fuel cell DC boost converter; η_{fc}—fuel cell efficiency, which depends on the fuel cell output power; and LHV—hydrogen lower heating value [J/kg].

Equation (26) can be expressed in terms of the hydrogen consumption function (Figure 3), described by the quadratic function given in Equation (10). Therefore, the equivalent hydrogen consumption due to battery power is

$$\dot{m}_{bat} = \begin{cases} f\left(\dfrac{P_{bat}}{\eta_{ch}\cdot\eta_{dsch}\cdot\eta_{dc}}\right) & P_{bat} \geq 0 \\[3mm] f\left(\dfrac{P_{bat}\cdot\eta_{ch}\cdot\eta_{dsch}}{\eta_{dc}}\right) & P_{bat} < 0 \end{cases} \tag{27}$$

The objective function to be minimized is described as follows:

$$J\left(P_{bat}, P_{fc}\right) = \min \dot{m}_{eqv}(t) \tag{28}$$

The constraints that should be taken into account are

$$
\begin{cases}
P_{bat} + P_{fc} = P_{req} \\
SOC_{\max} > SOC > SOC_{\min} \\
P_{fc,\max} > P_{fc} > P_{fc,\min} \\
P_{bat,\max} > P_{bat} > P_{bat,\min}
\end{cases}
\tag{29}
$$

The values of the parameters, used in the ECMS control strategy, are provided in Table 4.

Table 4. Parameters for ECMS control strategy.

| Parameters	Label	Unit	Value
Desired state of charge	SOC_t	%	60
Maximum state of charge	SOC_{max}	%	70
Minimum state of charge	SOC_{min}	%	45
Power coefficient	k_s	-	3
Battery charging efficiency	η_{ch}	-	0.9
Battery discharging efficiency	η_{dsch}	-	0.9
DC boost converter efficiency	η_{dc}	-	0.95
Hydrogen lower heating value	LHV	MJ/kg	120
Fuel cell minimum power	$P_{fc,min}$	kW	0
Fuel cell maximum power	$P_{fc,max}$	kW	113
Battery minimum power	$P_{bat,min}$	kW	−20
Battery maximum power	$P_{bat,max}$	kW	20

4.2. Simulation Results with ECMS

The performance of ECMS control strategy on the Toyota Mirai FCHEV along with numerical findings on the advantages in terms of hydrogen consumption with respect to rule-based and real control strategies are evaluated in this section. Figure 9 presents the graphical representation of FC power, current, hydrogen flow rate, battery power, current, and SOC for WLTC driving cycle and three different control strategies. Blue and yellow lines show modeled and optimized data, whereas the red line shows experimental data.

The final battery SOC values for three different controllers over six different driving cycles are shown in Table 5. These data are required to calculate the correct hydrogen adjustment for the objective comparison of fuel consumption. Since the SOC lower limit constraint was set at 45%, the final values of the battery SOC for the ECMS controller typically differ greatly from modeled and experimental ones. Therefore, the state of charge at the beginning and end of the simulation is equalized by correcting SOC with the corresponding amount of hydrogen. Moreover, Table 5 represents the numerical values of hydrogen consumption in grams for rule-based, real and optimized ECMS control strategies over WLTC, NEDC, UDDS, JC08, US06 and HWY driving cycles. In comparison to the real control technique, the results obtained show that by adopting ECMS, the maximum hydrogen consumption decrease of more than 15% is attained for WLTC, US06, and HWY driving cycles. For WLTC, compared with the rule-based and real strategies, almost the same consumption reduction of about 15% is observed, whereas 11.5% with respect to rule-based and 17.5% to real control strategies are estimated for the US06 cycle. Concerning the HWY cycle, ECMS offers approximately 20% of the advantage with respect to the real control strategy, while just 4.2% regarding the rule-based one. The ECMS comes out to perform worse than real controllers for the NEDC, UDDS, and JC08 driving cycles, with a contrary effect of fuel economy increases of up to 17.6% for the UDDS, 13.6% for the JC08, and 1.4% for the NEDC cycles, respectively. However, for all driving cycles, ECMS outperforms rule-based techniques, with a minimum advantage of 0.4% for UDDS and a maximum advantage of 15.6% for WLTC. This can be explained by the fact that the fuel cell system runs in zones with higher efficiency and that the average FC system efficiency with a real controller over UDDS, NEDC, and JC08 is higher than with an ECMS controller. Figure 10, which shows the time history of FC system efficiency over UDDS driving cycles for three different EMS, clearly illustrates this point. The NEDC and JC08 driving cycles show a similar pattern. These findings support those found in Table 5. The real controller, shown by the red line in this plot, is situated above the rule-based and ECMS controllers,

represented by the blue and yellow lines. In addition, the blue and yellow lines nearly overlap, confirming that the simulated and experimental hydrogen consumption for the UDDS and JC08 cycles are almost identical. The results show that there is still potential to improve both the real and ECMS control strategies.
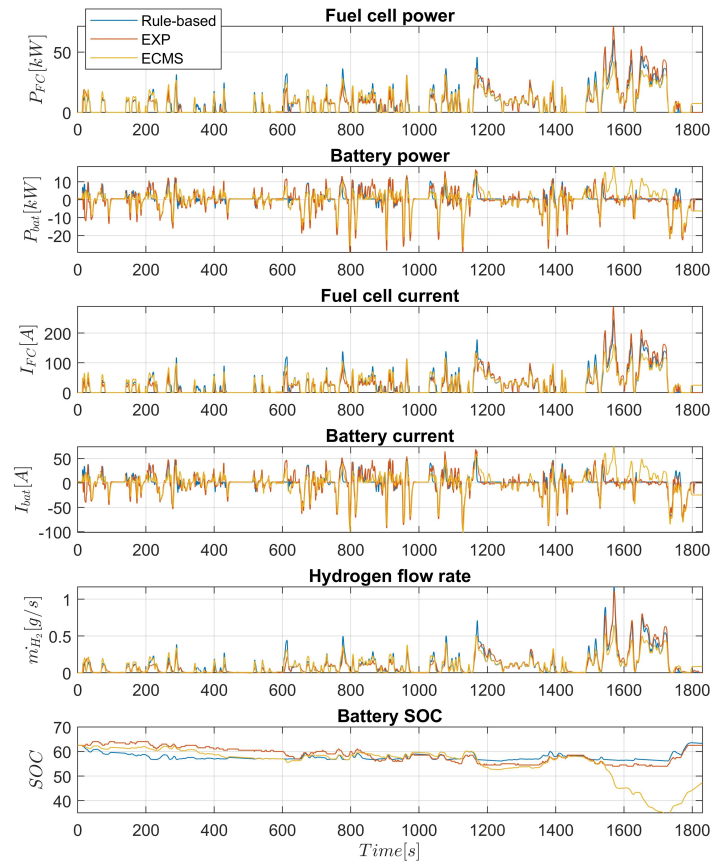
Figure 9. Simulation results for WLTC driving cycle with ECMS.
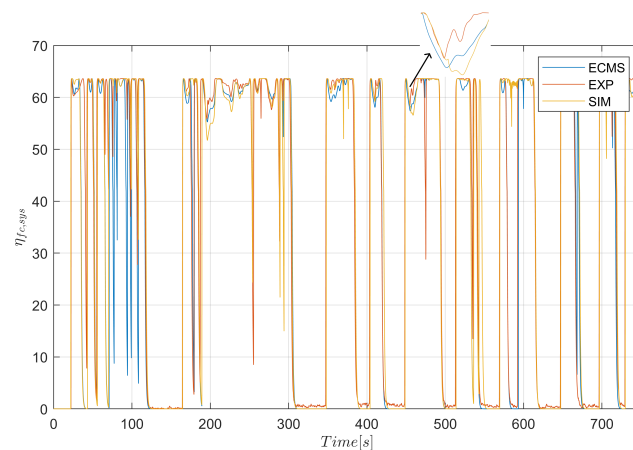
Figure 10. Fuel cell system efficiency for UDDS driving cycle.

Table 5. Simulation results for hydrogen consumption with ECMS.

	Hydrogen Consumption [g]							SOC [%]		
Drive Cycle	SIM (ECMS)	SOC Compensation	ECMS Total	Rule-Based Total	EXP	Economy (ECMS and Rule-Based)	Economy (ECMS and EXP)	SIM (Rule-Based)	EXP	SIM (ECMS)
WLTC	180.4	-13.4	166.8	197.7	197	−15.6%	−15.2%	63.29	62.5	47.39
NEDC	167.5	-5	162.6	177.8	160	−8.6%	+1.4%	65.62	62.5	57
UDDS	90.36	-0.7	89.6	89.9	76.2	−0.4%	+17.6%	57.37	59	58.17
JC08	61.27	-0.7	60.6	62.8	53.3	−3.6%	+13.6%	59.89	59.5	58.72
US06	272.6	-6.2	266.4	301.2	323	−11.5%	−17.5%	62.74	57	50.15
HWY	197.4	-1.3	196.1	204.7	244	−4.2%	−19.6%	62	58.5	57.02

5. Conclusions

In this paper, a full MATLAB/Simulink model of the FCHEV has been developed and validated, simulating all vehicle components over several driving cycles. This model has been found to be rapid and to produce results that are reliable and steady. In order to determine the ideal power split between the fuel cell and battery, an ECMS control method for fuel cell vehicles was developed and put to the test in the Toyota Mirai FCHEV. The design of the FCHEV energy management strategy involved reconstructing the experimental EMS using a linear regression approach and approximating it with rules-based EMS, which consists of six distinct modes of operation. For the WLTC cycle, the modeled and experimental data matched perfectly with a difference of just 0.5%, whereas the UDDS and HWY driving cycles had the largest differences of nearly 18% and 16%, respectively. In conclusion, this model performs well for low-load driving cycles such as WLTC, NEDC, JC08, and US06, with an error of less than or about equal to 10%.

The ECMS control strategy has been simulated in the Toyota Mirai FCHEV to optimize the power split between power sources. Instantaneous fuel cell and equivalent battery hydrogen consumptions have been calculated from an approximated hydrogen consumption polynomial. The penalty function that incorporates battery SOC was taken into account while defining the objective function. For all driving cycles, it was found that the ECMS controller outperforms the rule-based strategy, with a minimum fuel consumption reduction of 0.4% for UDDS and a maximum of 15.6% for WLTC. The ECMS controller, on the other hand, proves to perform worse than a real controller for NEDC, UDDS, and JC08 cycles, with a contrary effect of fuel economy, increasing up to 17.6% for UDDS, 13.6% for JC08, and 1.4% for NEDC cycles, while the fuel economy reduction was observed to be 15.2%, 17.5%, and 19.6%, respectively, for the WLTC, US06, and HWY driving cycles. The temperature of the components affects the performance of the powertrain, which can be considered in future work.

Abbreviations

The following abbreviations are used in this manuscript:

FCHEV	Fuel cell hybrid electric vehicle
FCEV	Fuel cell electric vehicle
ECMS	Equivalent consumption minimization strategy
ANL	Argonne national laboratory
ICE	Internal combustion engine
FC	Fuel cell
BEV	Battery electric vehicle
EMS	Energy management strategy
SOC	State of charge
HEV	Hybrid electric vehicle
UDDS	Urban dynamometer driving schedule
WLTC	Worldwide harmonized Light vehicles Test Cycles
NEDC	New European Driving Cycle
EM	Electric machine
NiMH	Nickel Metal Hydride
OCV	Open circuit voltage
LHV	Lower heating value

References

1. Sources of Greenhouse Gas Emissions. EPA United States Environmental Protection Agency Report. 2019. Available online: https://www.epa.gov/ghgemissions/sources-greenhouse-gas-emissions (accessed on 10 March 2023).
2. Gurney, J.; Company, B. BP Statistical Review of World Energy. *J. Policy Anal. Manag.* **1985**, *4*, 283.
3. Ajanovic, A.; Haas, R. Economic and Environmental Prospects for Battery Electric- and Fuel Cell Vehicles: A Review. *Fuel Cells* **2019**, *19*, 515–529.
4. Bazarov, B.; Magdiev, K.; Akhmatjanov, F.; Sidikov, F.; Vasidov, B.; Usmanov, I. Assessment of environmental and energy usage of alternative motor fuels. *Asia-Pac. Conf. Appl. Math. Stat.* **2022**, *2432*, 020001.
5. Castellazzi, L.; Ruzimov, S.; Bonfitto, A.; Tonoli, A.; Amati, N. A Method for Battery Sizing in Parallel P 4 Mild Hybrid Electric Vehicles. *SAE Int. J. Electrified Veh.* **2021**, *11*, 97–111.
6. Jayakumar, A.; Madheswaran, D.; Kannan, A.; Sureshvaran, U.; Sathish, J. Can hydrogen be the sustainable fuel for mobility in India in the global context? *Int. J. Hydrogen Energy* **2022**, *47*, 33571–33596. https://doi.org/10.1016/j.ijhydene.2022.07.272.
7. Manoharan, Y.; Hosseini, S.E.; Butler, B.; Alzahrani, H.; Foua, B.; Ashuri, T.; Krohn, J. Hydrogen Fuel Cell Vehicles; Current Status and Future Prospect. *Appl. Sci.* **2019**, *9*, 2296.
8. Garland, N.L.; Papageorgopoulos, D.C.; Stanford, J.M. Hydrogen and Fuel Cell Technology: Progress, Challenges, and Future Directions. *Energy Procedia* **2012**, *28*, 2–11.
9. Li, W.; Feng, G.; Jia, S. An Energy Management Strategy and Parameter Optimization of Fuel Cell Electric Vehicles. *World Electr. Veh. J.* **2022**, *13*, 21.
10. Tanç, B.; Arat, H.; Baltacioğlu, E.; Aydin, K. Overview of the next quarter century vision of hydrogen fuel cell electric vehicles. *Int. J. Hydrogen Energy* **2018**, *44*, 10120–10128.
11. Thomas, C. Fuel cell and battery electric vehicles compared. *Int. J. Hydrogen Energy* **2009**, *34*, 6005–6020.
12. Khaligh, A.; li, Z. Battery, Ultracapacitor, Fuel Cell, and Hybrid Energy Storage Systems for Electric, Hybrid Electric, Fuel Cell, and Plug-In Hybrid Electric Vehicles: State of the Art. *Veh. Technol. IEEE Trans.* **2010**, *59*, 2806–2814.
13. Ostadi, A.; Kazerani, M. A Comparative Analysis of Optimal Sizing of Battery-Only, Ultracapacitor-Only, and Battery—Ultracapacitor Hybrid Energy Storage Systems for a City Bus. *IEEE Trans. Veh. Technol.* **2014**, *64*, 4449–4460.
14. Carello, M.; de Carvalho Pinheiro, H.; Longega, L.; Di Napoli, L. Design and Modelling of the Powertrain of a Hybrid Fuel Cell Electric Vehicle. *SAE Tech. Pap. Ser.* **2021**, *3*, 2878–2892.
15. Jayakumar, A.; Chalmers, A.; Lie, T.T. Review of prospects for adoption of fuel cell electric vehicles in New Zealand. *IET Electr. Syst. Transp.* **2017**, *7*, 259–266. https://doi.org/10.1049/iet-est.2016.0078.
16. Davis, S.; Williams, R.B.; Moore, S. *2016 Vehicle Technologies Market Report*; Oak Ridge National Laboratory: Oak Ridge, TN, USA, 2016.
17. Yakhshilikova, G.; Ezemobi, E.; Ruzimov, S.; Tonoli, A. Battery sizing for mild P2 HEVs considering the battery pack thermal limitations. *Appl. Sci.* **2022**, *12*, 226.
18. Onori, S.; Serrao, L.; Rizzoni, G. *Hybrid Electric Vehicles Energy Management Strategies*, 1st ed.; Springer: Berlin/Heidelberg, Germany, 2016.
19. Fleuren, M.; Romijn, T.; Donkers, M. An Equivalent Consumption Minimisation Strategy based on 1-Step Look-Ahead Stochastic Dynamic Programming. *IFAC-PapersOnLine* **2015**, *48*, 72–77.
20. Liu, Y.; Zhu, L.; Tao, F.; Fu, Z. Energy management strategy of FCHEV based on ECMS method. In Proceedings of the 2019 8th International Conference on Networks, Communication and Computing, Toronto, ON, Canada 2019; pp. 197–201.
21. Paganelli, G.; Delprat, S.; Guerra, T.M.; Rimaux, J.; Santin, J.J. Equivalent consumption minimization strategy for parallel hybrid powertrains. *IEEE Veh. Technol. Conf.* **2002**, *4*, 2076–2081.

22. Paganelli, G.; Guezennec, Y.; Rizzoni, G. Optimizing Control Strategy for Hybrid Fuel Cell Vehicle. *SAE Trans.* **2002**, 398–406.

23. Han, J.; Park, Y.; Kum, D. Optimal adaptation of equivalent factor of equivalent consumption minimization strategy for fuel cell hybrid electric vehicles under active state inequality constraints. *J. Power Sources* **2014**, *267*, 491–502.

24. Bassam, A.; Phillips, A.; Turnock, S.; Wilson, P. An improved energy management strategy for a hybrid fuel cell/battery passenger vessel. *Int. J. Hydrogen Energy* **2016**, *41*, 22453–22464.

25. Li, H.; Ravey, A.; N'diaye, A.; Djerdir, A. Equivalent consumption minimization strategy for fuel cell hybrid electric vehicle considering fuel cell degradation. In Proceedings of the 2017 IEEE Transportation Electrification Conference and Expo (ITEC), Chicago, IL, USA, 22–24 June 2017; 540–544.

26. Kamal, E.; Adouane, L. Optimized EMS and a Comparative Study of Hybrid Hydrogen Fuel Cell/Battery Vehicles. *Energies* **2022**, *15*, 738.

27. Lohse-Busch, H.; Duoba, M.; Stutenberg, K.; Iliev, S.; Kern, M.; Richards, B.; Christenson, M.; Loiselle-Lapointe, A. *Technology Assessment of a Fuel Cell Vehicle: 2017 Toyota Mirai*; Report #ANL/ESD-18/12; U.S. Department of Energy, Fuel Cell Technologies Office: Argonne, IL, USA, 2018.

28. D3 2016 Toyota Mirai. Toyota Mirai Argonne National Laboratory Testing Results. 2019. Available online: https://www.anl.gov/taps/d3-2016-toyota-mirai (accessed on 10 March 2023).

29. Outline of the Mirai. 2017. Available online: www.toyota-europe.com (accessed on 10 March 2023).

30. Usmanov, U.; Yuldashev, Q. State of the art of fuel cell technology in automotive industry. *Int. J. Universum Tech. Sci.* **2022**, *5-11*, 33–40.

31. Usmanov, U. Control Strategy Optimization of Toyota Mirai Based Fuel Cell Hybrid Electric Vehicles. Master's Thesis, Politecnico di Torino, Turin, Italy 2022.

32. Guzzella, L.; Sciarretta, A. *Vehicle Propulsion Systems: Introduction to Modeling and Optimization*; Springer: Berlin/Heidelberg, Germany, 2007.

33. Mukhitdinov, A.; Ruzimov, S.; Eshkabilov, S. Optimal Control Strategies for CVT of the HEV during a regenerative process. In Proceedings of the 2006 IEEE Conference on Electric and Hybrid Vehicles, ICEHV, Pune, India, 18–20 December 2006; pp. 1–12.

34. Toyota Mirai Technical Specifications vs. FCHV, November 2014. Available online: https://mag.toyota.co.uk/toyota-mirai-technical-specifications-vs-fchv-adv/ (accessed on 10 March 2023).

35. YASA P400R SERIES Electric Machine Datasheet. Available online: https://www.yasa.com/products/yasa-p400/ (accessed on 10 March 2023).

36. Mavlonov, J.; Ruzimov, S.; Tonoli, A.; Amati, N.; Mukhitdinov, A. Sensitivity Analysis of Electric Energy Consumption in Battery Electric Vehicles with Different Electric Motors. *World Electr. Veh. J.* **2023**, *14*, 36.

37. Luciani, S.; Tonoli, A. Control Strategy Assessment for Improving PEM Fuel Cell System Efficiency in Fuel Cell Hybrid Vehicles. *Energies* **2022**, *15*, 6.

38. Idaho National Laboratory. Department of Energy Advanced Vehicle Testing. 2004 Toyota Prius—1052 Hybrid Battery Test Results. Available online: https://avt.inl.gov/sites/default/files/pdf/hev/batteryprius1052.pdf (accessed on 10 March 2023).

39. Wu, G.; gui Lu, R.; Zhu, C.; Chan, C.C. Apply a Piece-wise Peukert's Equation with Temperature Correction Factor to NiMH Battery State of Charge Estimation. *J. Asian Electr. Veh.* **2010**, *8*, 1419–1423.

40. Kenneth, K.; Mark, M.; Matthew, Z. Battery usage and thermal performance of the Toyota Prius and Honda Insight during chassis dynamometer testing. XVII. In Proceedings of the The Seventeenth Annual Battery Conference on Applications and Advances, Long Beach, CA, USA, 18 January 2002.

41. Prodeep, D.J.; Noel, M.M.; Arun, N. Nonlinear control of a boost converter using a robust regression-based reinforcement learning algorithm. *Eng. Appl. Artif. Intell.* **2016**, *52*, 1–9.